IEEE Access
Multidisciplinary | Rapid Review | Open Access Journal

Received July 26, 2018, accepted September 3, 2018, date of publication September 10, 2018, date of current version October 12, 2018.

Digital Object Identifier 10.1109/ACCESS.2018.2869138

Sparsity Enhanced Topological Fractal Decomposition for Smart Machinery Fault Diagnosis

XINCHENG CAO[1], NIANYIN ZENG[1], (Member, IEEE), BINQIANG CHEN[1], AND WANGPENG HE[2], (Member, IEEE)

[1]School of Aerospace Engineering, Xiamen University, Xiamen 361005, China
[2]School of Aerospace Science and Technology, Xidian University, Xi'an 710071, China

Corresponding author: Binqiang Chen (cbq@xmu.edu.cn)

This work was supported in part by the National Natural Science Foundation of China under Grant 51605403, in part by the Natural Science Foundation of Guangdong Province, China, under Grant 2015A030310010, in part by the Natural Science Foundation of Fujian Province, China, under Grant 2016J01012, in part by the Natural Science Foundation of Shaanxi Province of China under Grant 2018JQ5106, and in part by the CAST-BISEE Innovation Fund under Grant CAST-BISEE2017-008.

ABSTRACT Automatic fault feature extraction-based smart fault diagnosis is becoming more and more popular, as it does not require excessive expertise of on-site staff. Advanced signal processing techniques are of significant importance in order to ensure efficient and effective fault feature analysis. Multi-resolution analysis is an effective tool utilized to decouple multiple signal modes within the measured vibration signal. However, current multi-resolution analyzing methods still cannot enable continuous spectral refinements around fixed analyzing frequencies. To address this problem, a novel theory of topological fractal multi-resolution analysis (TFMRA) is proposed. With the concept of nested centralized wavelet packet cluster (NCWPC), TFMRA is equipped with the ability to extract multiple fault features simultaneously. Mathematically, we prove that: 1) each NCWPC is a topology subset of spectral domain of the investigated signal and 2) all sets of NCWPC share a common self-similar fractal property in geometry. This paper reveals an important intrinsic relation between classical dyadic multi-resolution analysis and TFMRA. That is, each dyadic wavelet packet can be uniquely associated with an NCWPC according to the definitions of TFMRA, and classical wavelet packet spaces are regarded as proper subsets of the proposed NCWPCs. Combining signal decomposition using TFMRA and damage information of a mechanical system, we propose an improved sparsity promoted vibration signature analyzing methodology to investigate repetitive transient fault features. This method was applied to extract abnormal vibration signatures from an experimental rotor test rig with rub-impact faults. Processing results demonstrate that nanocomponents of transient vibrations, which are produced by rub-impact faults, were successfully identified. These results are compared with those of some other comparison techniques based on sparse representation. It is verified that the proposed fault diagnosis method possesses more robust noise resisting capability.

INDEX TERMS Rotating machinery, fault diagnosis, topology fractal multi-resolution analysis (TFMRA), sparse representation, rub-impact.

I. INTRODUCTION

Rotating machinery plays an important role in modern industry, such as aeronautical and space technologies, mechanical manufacturing, power and energy, transpiration and etc. However, owing to harsh working conditions, such as heavy load, high temperature, as well as corrosive environment, mechanical faults are likely to occur on the components of rotating machinery. Without timely fault diagnosis services and effective maintenances, these faults not only affect the service performances of equipment but also result in fatal accidents causing major economic losses and severe casualties [1], [2]. Attempting at avoiding such accidents, predictive maintenance together with health prognosis techniques are indispensable. Dynamic signals, acquired during condition monitoring of rotating machinery, are feasible vehicles carrying important information of abnormal faults.

Extracting fault features from masking interferences has been recognized as a difficult problem of general interest in the community [3], [4].

The past decades have witnessed the rapid development of signal representation theory. This theory has been widely used in weak feature extraction of dynamic signals, in which vibration modes have distinct spectral counterparts. In order to enhance representing ability of non-stationarity, nonlinearity within dynamic signals, special bases should be carefully and properly chosen. Some related techniques are redundant trigonometric bases [5], wavelet transform [6], [7], self-adaptive signal decompositions [8], [9]. Empirical mode decomposition (EMD) and its later variations are well-known examples of the self-adaptive signal decomposition techniques. These famous methodologies are continuously finding more applications in fields of fault diagnosis and health prognosis [10]–[14]. Sparse representation (SR) is a relative recent enhancement to signal representation theory. In the framework of sparse representation, the bases mentioned above are examples of analyzing dictionaries [15], [16]. Techniques based on sparse representation are intensively investigated by researchers and they were applied in numerous machine health prognosis applications [17]–[22].

Wavelet analysis is an important tool of time-scale analysis. Until now, many wavelet systems have been developed according to diversified demands. However, no matter orthonormal bases, biorthogonal bases, dual-tree complex bases, or multi-wavelet bases, patterns of frequency-scale paving of these available discrete wavelet transforms are identical and fixed. Mathematically, they can realize refinement with regard to spectral resolution of wavelet subspaces, but each wavelet subspace is equipped with a unique central analyzing frequency different from that of the others. Moreover, they were reported to possess poor performance in analyzing transition band features [23]. On the other hand, self-adaptive signal decomposition techniques with artificial intervention, such as noise assisted ensemble EMD, variational mode decomposition are also of wavelet like filtering properties [24], [25]. Therefore, shortcomings of classical discrete wavelet theory also exist for these methods.

As stated above, different signal bases are employed to match vibration modes with specific characteristics. The idea of using multiple bases simultaneously to separate vibration components of distinguished characteristics via optimization have been investigated by many scholars. Cai *et al.* [26] and He *et al.* [27] explored some unconventional wavelet dictionaries, such as overcomplete framelet expansion, tunable quality-factor wavelet transform (TQWT), and super wavelet in mechanical fault feature extraction. These novel wavelet dictionaries adopt non-dyadic dilation factors and therefore enable frequency-scale paving patterns different from dyadic wavelet system. However, they are still not able to realize multi-resolution analysis around fixed spectral focuses. As such, in an advanced sparse representation algorithm, due to employment of multiple redundant dictionaries, more iterations are required and thus the resulting computation efficiency is low.

To achieve the merit of centralized multiresolution analysis, Chen investigated a derived ensemble analytic framelet expansion (DEAFE) based on dual tree wavelets. This redundant framelet expansion was reported to be an elegant way to solve the mentioned problem [28], [29]. However, it these researches, mathematical backgrounds regarding topological structures hidden in the DEAFE were not explained in a systematic way. Serving as further investigations of DEAFE, we proposed a novel theory of topological fractal multi-resolution analysis (TFMRA) with concrete construction example in this paper. The contribution in the theoretical aspect lies in topological structure explanation of DEAFE from viewpoints of point set topology theory. With rigorous mathematical proofs, the unique centralized multiresolution properties are revealed and a novel generalized theory of topology fractal multi-resolution analysis (TFMRA) is established.

Moreover, a smart fault feature extraction method is put forward based on TFMRA. In the diagnosis algorithm, a new sparsity estimation indicator was designed based on the periodic sparsity in the domain of envelope spectrum. This indicator can effectively distinguish periodic impulsive components even in the presence of masking noises as well as other types of interference. Using this indicator, parameters of optimal subspace can be properly selected. The NCWPC containing this optimal subspace and neighboring wavelet subspaces of this NCWPC are further investigated to detect incipient fault features. With derived information of instantaneous amplitude and instantaneous frequency, vibration modes with more complete physical meaning can be retrieved. Processing results of this fault diagnosis algorithm were compared with those of some other comparison methods based on sparse representation, such as group sparsity technique and TQWT based resonance sparsity decomposition, to verify its superiority of effectiveness.

II. CONCRETE EXAMPLE OF FRACTAL TOPOLOGICAL MULTI-RESOLUTION ANALYSIS

A. FUNDAMENTALS OF CLASSICAL DYADIC WAVELET THEORY

Subspaces of classical discrete wavelet theory are generated by a single scaling function and a single wavelet function. Let the sample frequency of digital discretization during machine health monitoring be denoted as f_s. As demonstrated in Figure 1, the spectral resolutions of wavelet packets $wp_j^k (j \in \mathbb{Z}^+ \cup \{0\}, k \in \mathbb{Z})$ are continuously enhanced by a factor of 2. While the central analyzing frequency (CAF) of wp_j^k can be computed as

$$CF_{j,k} = \frac{k+1}{2^{j+2}} f_s. \tag{1}$$

As shown, $\varphi : (j,k) \mapsto CF_{j,k}$ can be regarded as a mathematical mapping represented by $\mathbb{Z}^2 \mapsto \mathbb{R}$. It can be inferred that each wavelet packet (WP) possesses a unique

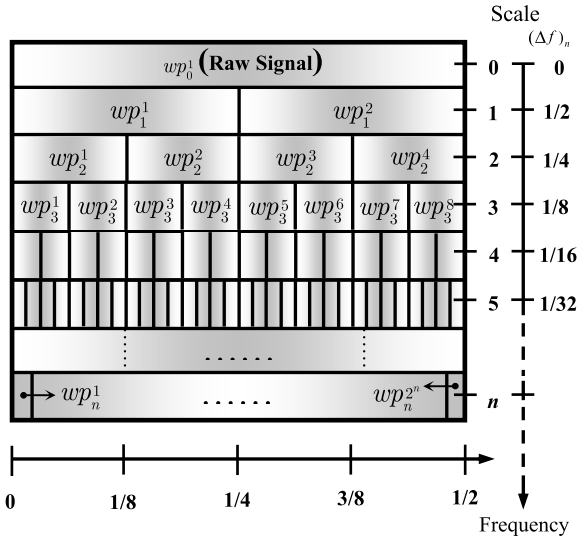

FIGURE 1. Frequency-scale paving pattern of the classical wavelet packet transform.

CAF that is different from that of other WPs. However, owing to the fact that the shape of wavelet spectral response is not ideally rectangular, WP has relatively poor performance in extracting dynamic features whose spectral responses are located at either end of passing-bands. That is, as a celebrated mathematical microscope, classical dyadic wavelet transform can achieve refined improvement of spectral resolution but actually cannot achieve multi-resolution analysis around some specific spectral focuses. Recent developments of overcomplete wavelet transform were designed to be equipped with flexible scaling factors as well as flexible CAFs. Unfortunately, the aim of centralized multiresolution analysis is still not achieved.

B. CONSTRUCTION OF IMPLICIT ENSEMBLE WAVELET TOPOLOGY FRCATAL DECOMPOSITION

In order to improve time-frequency localizability on the transition bands of current discrete wavelet analysis. In [26], a novel strategy for constructing implicit wavelet packet (IWP) was proposed. Routines of this strategy can be summarized in Algorithm 1.

C. MATHEMATICAL DESCRIPTION OF CENTRALIZED MULTIRESOLUTON ANALYSIS

In Figure 2, the frequency-scale paving pattern of the generated IWPs is illustrated. According to the definition in the above equations, for $k \geq 2$, the spectral responses of wavelet packet series $D_{k,j}^{(\cdot)}(n)$ can be written as

$$W_{k,j}^{(\cdot)}(w) = H_{1,b_1}^{(\cdot)}(w)\left(\prod_{u=2,u>k}^{i_{one}} H_{b_m}^{(\cdot)}(2^u w)\right) \times \left(\prod_{v=i_{one}+1,v>k}^{k} F_{b_v}(2^v w)\right), \quad (8)$$

Algorithm 1 IWP Construction Strategy

Input: $\boldsymbol{x} \in \mathbb{R}^N$

Step 1). Perform quasi-analytic wavelet packet transform (QAWPT) on the input signal $\boldsymbol{x}$ and implement single branch reconstructions for each wavelet packet series. Mapping between the input and the output can be expressed as

$$x \mapsto \{D_J^i | i = 1, 2 \cdots, 2^J\}, \quad (2)$$

where D_J^i denotes the reconstructed signal after inverse transform and J denotes the decomposition depth.

Step 2). Rearrange the order of elements in the set $\{D_k^i | i = 1, 2 \cdots, 2^k\}$, such that in the rearranged set $\{R_k^i | i = 1, 2 \cdots, 2^k\}$ the relation $CAF(R_k^l) < CAF(R_k^{l+1})$ exists for all $1 \leq l \leq 2^k$.

Step 2.1) For each wavelet packet $R_k^i(n)$ in the rearranged set, compute the binary coding for its index i, expressed as

$$i = \sum_{m=0}^{k-1} 2^m n_m + 1, \quad (3)$$

Step 2.2) Introduce an integer mapping $\varphi : \mathbb{Z}^+ \mapsto \mathbb{Z}^+$ for the coding $\{n_1, n_2, \ldots, n_m\}$. The definition of the mapping is defined as

$$\tilde{n}_m = \begin{cases} n_m, & m = k-1 \\ \mathrm{mod}(n_m + n_{m+1}, 2), & m = 0, 1, \cdots, k-2. \end{cases} \quad (4)$$

As such, a new integer $\tilde{i}$ can be defined as

$$\tilde{i} = \sum_{m=0}^{k-1} 2^m \tilde{n}_m + 1. \quad (5)$$

Step 2.3). According to the introduced mapping $\varphi\ (\mathbb{Z}^+)$:$i \mapsto \tilde{i}$, the relations between elements of the original set and those of the resultant set can be expressed as

$$R_k^i(n) \stackrel{def}{=} D_k^{\tilde{i}}(n). \quad (6)$$

Step 3). Engender implicit wavelet packets, shown as

$$IWP_{k-1}^i(n) = R_k^{2i}(n) + R_k^{2i+1}(n) \quad 2 \leq k, \quad 1 \leq i \leq 2^{k-1} - 1 \quad (7)$$

Output: $\{R_k^i(n)\} \in \mathbb{R}^N$ and $\{IWP_k^i(n)\} \in \mathbb{R}^N$.

where the binary coding for the integer j is expressed as

$$j = \sum_{i}^{k} b_i \cdot 2^{k-1-j}. \quad (9)$$

In the above equation, i_{one} indicates the first element belonging to the set $B_{k,j} = \{b_1, b_2, \ldots, b_k | b_{(\cdot)} = 0 \text{ or } 1\}$ that satisfies the following requirements in Equation (10).

$$\begin{cases} b_{i_{one}} = 1 \\ \sum_{i=2}^{n_{one}-1} b_i = 0 \end{cases} \quad (10)$$

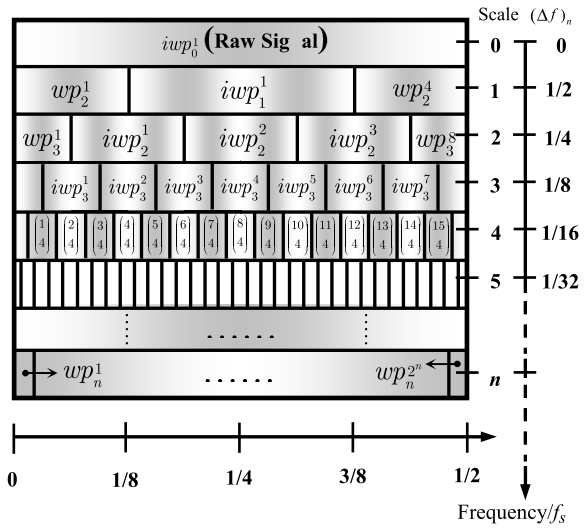

FIGURE 2. Frequency-scale paving pattern of the IWPs.

Let $\psi_{k,j}^e(t)$ be the impulse response function associated with $IWP_k^i(n)$, $\mathcal{EV}_{k,j}$ be the abstract sub-space generated by the translations of, and $\mathcal{R}_{k,i}$ be the sub-space generated by the dual tree wavelet functions $\{\psi_{k,i}^{\mathbb{C}}(t)\}$. According to the paving pattern shown in Figure 2, the following properties for the TFMRA can be summarized.

(1) $\{0\} \cdots \subset \mathcal{EV}_{k+1,4j} \subset \mathcal{EV}_{k,2j} \subset \mathcal{EV}_{k-1,j} \subset \cdots \subset L^2(\mathbb{R})$;

(2) $\lim_{k\to+\infty} \cup_{j\in\{1,\ldots,2^{j-1}-1\}} \mathcal{EV}_{k,j} = L^2(\mathbb{R})$;

(3) $x(t) \in \mathcal{EV}_{k,2j} \Leftrightarrow x(2t) \in \mathcal{EV}_{k-1,j}, \forall\, (k,j) \in \mathbb{Z}^2$;

(4) For arbitrary $(k,j,m) \in \mathbb{Z}^3$, there is an equivalent relation shown as below

$$f(t) \in \mathcal{EV}_{k,j} \;\Leftrightarrow\; f(t - 2^{k-1}\cdot m) \in \mathcal{EV}_{k,j};$$

(5) For $\forall\, j \in \mathbb{Z}$, the relation $\mathcal{EV}_{j+1,i} = \mathcal{R}_{j,2i} \oplus \mathcal{R}_{j,2i+1}$ can be satisfied;

(6) $\lim_{k\to+\infty} \bigcap_{j\in\{1,\ldots,2^{j-1}-1\}} \mathcal{EV}_{k,j} = L^2(\mathbb{R})$.

To make formal descriptions of the special properties of TFMRA, a novel concept of nested centralized wavelet packet cluster is proposed with definitions.

Definition 1 (Topological Fractal Multi-Resolution Analysis, TRMRA):

(1) Nested centralized wavelet packet cluster (NCWPC), defined as:

For $\forall\, j = 1, 2, \ldots, 2^k$ and $k \geq 2$, the order of an element in an NCWPC is determined by the value of the index k:

$$NCWPC_{k,j}\{CAF_{k,j},\ \Delta f_k\} = \{\psi_{k',j'}^e(t)|\ k' \geq k,\ j' = 2^{k'}\}, \tag{11}$$

where $CAF_{k,j} = f_s/2^{k+1} + (j-1)\cdot\Delta f_k$ denotes the shared central analyzing frequency of a NCWPC and $\Delta f_k = f_s/2^k$ denotes the passing band width of the first element in the set $NCWPC_{k,j}$;

(2) Augmented nested centralized wavelet packet cluster (ANCWPC), defined as

$$ANCWPC_{k,j} = \{\psi_{k-1,j}\} \cup NCWPC_{k,j}, \tag{12}$$

(3) Nested centralized topological set

$$\overline{ANCWPSC_{k,j}} = \emptyset \cup ANCWPSC_{k,j} \cup \{[0, f_s/2]\}. \tag{13}$$

In the above definitions, $ANCWPC_{k,j}$ is called as the principal part of $\overline{ANCWPC_{k,j}}$.

(4) The passing band of $\psi_{k,j}^e(t)$ is

$$\left[\frac{2j-1}{2^{k+2}}, \frac{2j+1}{2^{k+2}}\right] f_s. \tag{14}$$

It can also be named as the support of $\psi_{k,j}^e(t)$, which can be expressed as $\mathrm{supp}(\psi_{k,j}^e)$ or $\mathrm{supp}_{k,j}(i)$. ■

More detailed introductions about these concepts and definitions will be addressed in the following parts.

III. FUNDAMENTAL THEORY OF TOPOLOGICAL FRACTAL MULTIRESOLUTION ANALYSIS

In this section, we attempt to illustrate special characteristics of TFMRA from viewpoints of filers, algebra, as well as geometry. In order to reveal the intrinsic properties of frequency-scale paving pattern generated by IWPs, the diagram in Figure 2 is equivalently expressed in Figure 3. As marked in the right side of the paving pattern in Figure 3, the height of each scale is reduced by a factor of 2 iteratively (such as '1', '1/2', '1/4', '1/8', and etc). However, in viewing of visual convenience, they are plotted with an identical height.

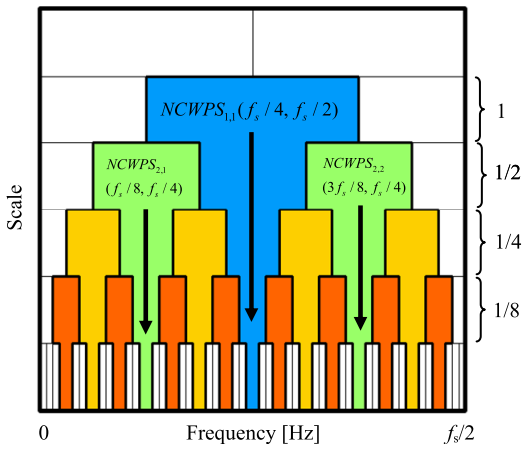

FIGURE 3. An equivalent expression of the frequency-scale paving pattern of the IWPs in Figure 2.

A. VERIFICATIONS OF PROPERTIES OF TFMRA

As illustrated in Figure 3, a J stage wavelet packet decomposition engenders 2^J wavelet packets. Moreover, $(2^{J-1}-1)$ additional IWPs are produced. Inferred form this diagram, the first set of nested centralized wavelet packet cluster, $NCWPS_{1,1}$, is produced at the stage of which $J = 2$.

While two sets of nested centralized wavelet packet cluster, $NCWPS_{2,1}$ and $NCWPS_{2,2}$, are generated at the stage of which $J = 3$. As such, we can make the following conclusions.

(1) All elements in a set of nested centralized wavelet packet cluster, $NCWPS_{k,j}$, share an identical CAF, while their spectral resolutions are continuously refined by a factor of 2.

(2) Comparing Figure 2 with Figure 3, wavelet packets, generated by a J stage dyadic decomposition, can be associated with implicit wavelet packets at the stage of $(J+1)$ due to their common spectral resolutions. It can be observed that 2^{J-2} new sets of NCWPS are produced at this stage .

(3) The initial element of $NCWPC_{k,j}$ is associated with the IWP function $\psi^e_{k,2j-1}(t)$. For successive elements in this set, the values of the indices also satisfy a dyadic scaling relation. That is, they can be denoted as $\{\psi^e_{k+k',(2j-1)\cdot 2^{k'}}(t)\}$ for $k' \geq 0$;

(4) Similar with the conventional dyadic wavelet packet transform, adjacent wavelet functions of the same NCWPC satisfy two-scale relationship approximately regarding their waveform shapes of impulse responses.

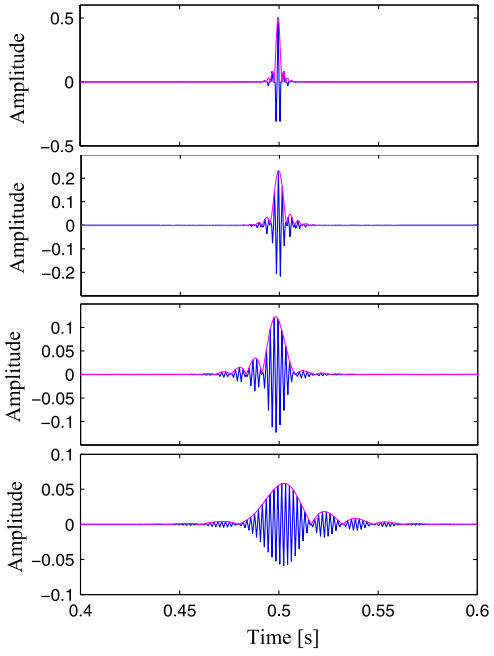

FIGURE 4. Time-frequency atoms of the first four IWPs of the set $\mathbf{NCWPC_{1,1}}$.

In order to make verifications of the above properties, in Figure 4 four wavelet functions of with their envelopes, belonging to the set of $NCWPC_{1,1}$, are plotted in the time domain. Observing from the waveforms, we find that each function consists of a main lobe and a few side lobes. On the other hand, their main lobes approximately satisfy the celebrated two-scale relationship in classical wavelet theory, although there are slight phenomena of asymmetry. According to the filtering structure of quasi-analytic wavelet packet theory [28], [29], the asymmetry is induced by the asymmetric orthonormal wavelet bases adopted at the first stage.

B. TOPOLOGICAL DESCRIPTION OF NCWPC COMBINED WITH SUBSPACE OF ORIGINAL SIGNAL

In theory of real analysis, definitions of topology space are shown in Dilemma 1.

Dilemma 1 (Topological Space, TS): A non-empty set X, together with a collection of open subsets $\mathfrak{D}$ is called a topological space, denoted as $(X, \mathfrak{D})$, if $\mathfrak{D}$ satisfy the following requirements:

(1) The empty set $\emptyset \in \mathfrak{D}$ and the original set $X \in \mathfrak{D}$;
(2) If $G_\alpha \in \mathfrak{D}(\alpha \in \mathcal{A})$, $\bigcup_{\alpha\in\mathcal{A}} G_\alpha \in \mathfrak{D}$;
(3) If $G_i \in \mathfrak{D},\ i = 1, 2, \ldots, n$, $\bigcap_{i=1}^{n} G_i \in \mathfrak{D}$. ■

In the frequency-scale paving pattern shown in Figure 3, according to the definitions of nested centralized topological set $\overline{ANCWPS_{k,j}}$, it is consolidated that the first requirement in Dilemma 1 is satisfied. Let a non-empty integer set $\mathcal{A}$ be denoted as

$$\mathcal{A} = \{i_1, i_2, \ldots | i_{(\cdot)} \in \mathbb{Z}^+ \cup \{0\}\}. \tag{15}$$

In this set, elements are sorted in numerical order. A nesting property exists as

$$\mathrm{supp}_{k,j}(i_1) \supset \mathrm{supp}_{k,j}(i_2) \supset \ldots \supset \mathrm{supp}_{k,j}(\lim_{\ell\to\infty} i_\ell), \tag{16}$$

where $\lim_{\ell\to\infty} i_\ell$ denotes the index of the last element in the set $\mathcal{A}$ (for finite geometry). The support of this element is $[CAF_{k,j} - \varepsilon, CAF_{k,j} + \varepsilon]$. The length of the support is so short that is can be regarded as a signal value equivalent to the CAFs of NCWPCs. As such, the following relations

$$\bigcup_{\alpha\in\mathcal{A}} ANCWPS_{k,j}(\alpha) = \mathrm{supp}_{k,j}(i_1) \in ANCWPS_{k,j}, \tag{17}$$

$$\bigcap_{\alpha\in\mathcal{A}} ANCWPS_{k,j}(\alpha) = \mathrm{supp}_{k,j}(\infty) \in ANCWPS_{k,j} \tag{18}$$

validate property (2) and property (3) in Dilemma 1. Based on the above arguments, it is sufficient to say that the constructed $ANCWPS_{k,j}$ are topological spaces according to strict mathematical definitions.

C. TOPOLOGICAL DESCRIPTION OF NCWPC

In Figure 3, the colored areas within the special trapezium-rectangle pattern (TRP) represent the supports of NCWPC. Observing the special TRPs indicated in this figure, we can conclude two essential properties.

(1) Two NCWPCs generated at adjacent scales, for example $\mathrm{NCWPC}_{1,1}$ and $\mathrm{NCWPC}_{2,1}$, are strictly similar in the geometric aspect. If we scale the shape of TRP associated with $\mathrm{NCWPS}_{2,1}$ by a factor of 2, the resultant shape is identical to that of the TRP associated with $\mathrm{NCWPC}_{1,1}$.

(2) A dyadic property also exists for numbers of NCWPC sets generated at adjacent scales. At the first scale, only one set ($\mathrm{NCWPC}_{1,1}$) is generated. While at the next scale, two new sets of NCWPC, $\mathrm{NCWPC}_{2,1}$ and $\mathrm{NCWPC}_{2,2}$, are produced. If arbitrary zoom-in operations are enabled for other TRPs in Figure 3, it can be inferred that the above phenomena also exist for other stages. Therefore, let this TRP be a basic geometrical pattern, it is feasible to conclude that the shapes of the generated NCWPCs are strictly similar with each

other geometrically. The mentioned TRPs can be employed to construct fractal sets in the frequency-scale plane.

IV. UNIFORM EXTENSION OF DYADIC WAVELET THEORY TO TOPOLOGICAL FRACTAL THEORY

Based on the presented materials, it is validated that theory TFRMA can be established using the concept of NCWPC. Geometrically, this claim can be reflected by the frequency-scale plane paved by TRPs of different scales. For classical dyadic wavelet theory, self-symmetry properties also exist for wavelet packets. However, the frequency-scale plane cannot be paved by geometric patterns in the framework of fractal theory. As a result, we manage to establish an essential relation between the proposed TFMRA and classical dyadic wavelet theory. This relation is defined by the following Theorem 1.

Theorem 1: Each dyadic wavelet packet can by uniquely associated with a specific NCWPC$_{k,j}$. Equivalently, a one-to-one mapping exists for dyadic wavelet theory and TFMRA.

Proof: For each dyadic wavelet packet $\mathcal{R}_{k,i}$, let its corresponding impulse response be denoted by $\psi_{k,j}(t)$. The CFA and the support of $\psi_{k,j}(t)$ are computed as

$$CAF\{\hat{\psi}_{k,j}(w)\} = \frac{2j-1}{2^{k+2}} f_s, \tag{19}$$

and

$$\text{supp}\{\hat{\psi}_{k,j}(w)\} = \left[\frac{j-1}{2^{k+1}}, \frac{j}{2^{j+1}}\right] f_s. \tag{20}$$

Comparing CAFs of dyadic wavelet packets with those of NCWPCs, we have the following equation

$$\frac{f_s}{2^{k'+1}} + (j'-1)\cdot\frac{f_s}{2^{k'}} = \frac{2j-1}{2^{k+2}} f_s. \tag{21}$$

Inferred from the identity, it is deduced that $k' = k+1$ and $j' = j$. On the other hand, the band width of the initial element of NCWPC$_{k+1,j}$ is $f_s/2^{k+2}$. It exactly equals one half of passing band width of $\hat{\psi}_{k,j}(w)$ in value. As such, there is an implicit one-to-one mapping revealed by the theory of TFMRA, which can be expressed as

$$\psi_{k,j} \mapsto NCWPS_{k+1,j}. \tag{22}$$

Without loss of generality, the wavelet space of the original signal $\boldsymbol{x}$ can be written as $\psi_{0,1}$, whose wavelet function is the Dirac impulse function $\delta(t)$. Equation (22)(22) reveals that each dyadic wavelet packet ($\psi_{k,j}$) can be uniquely associated with the set $NCWPC_{k+1,j}$. By adding $\psi_{k,j}$ to $NCWPC_{k+1,j}$, a generalize set NCWPC can be obtained without violating definitions of topology space. This is the reason why we propose the concept of ANCWPS in Definition 1.

According to the above arguments, except for the areas marked by the white color in Figure 3, there is a strict one-to-one mapping connecting classical dyadic wavelet theory and the proposed TFMRA. The former can be regarded as a special proper subset of the latter one. Equivalently, the novel multi-resolution theory is compatible with the classical one.

V. SMART FAULT FEATURE EXTRACTION BASED ON TFMRA

For rotating machinery operating at constant speed, the presence of localized faults developed on mechanical components will produce periodic impulsive transients in the vibration measurement. Inspired by the ideal of fault feature ratio (FFR) proposed by He *et al.* [27], we attempt to present an improved sparsity estimation indicator. Moreover, this indicator is combined with the proposed TFMRA to diagnose mechanical faults.

Let $\boldsymbol{x}$, the measured vibration signal, be the input of the proposed methodology. The flow chart of this smart diagnosis algorithm is illustrated as below.

Step 1). Compute characteristic frequencies of potential mechanical faults (f_c) based on information of machinery structure.

Step 2). Decompose the input signal $\{x(n)\}$ using the proposed TFMRA such that filtered signals of WPs and IWPs subspaces are obtained. These signals are represented as $\{\psi_{k,j}(n)\}$ and $\{\psi^e_{k,j}(n)\}$.

Step 3). Estimate the sparse indicators of these reconstructed signals.

Step 3.1) Firstly, compute the kurtosis value of each signal in the time domain, as shown in Equation (23)(23).

$$K[\psi^{(\cdot)}_{k,j}] = \frac{\mu_4}{\sigma^4} = \frac{E[(\psi^{(\cdot)}_{k,j} - \mu)^4]}{(E[(\psi^{(\cdot)}_{k,j} - \mu)^2])^2}, \tag{23}$$

where μ stands for the mean value of input signal; μ_4 stands for the fourth order moment of input signal; and σ stands for the standard deviation of input signal.

Step 3.2) Secondly, compute the kurtosis of the envelope of each wavelet series, denoted as $K_e[x(n)]$. The definition of $K_e[x(n)]$ is given as

$$K_e[x(n)] = K\left[\sqrt{x^2 + [\mathcal{H}\{x\}]^2}\right]. \tag{24}$$

where the operator $\mathcal{H}\{\cdot\}$ performs Hilbert transform on the input series. The definition of $\mathcal{H}\{\cdot\}$ are shown in Equation (25).

$$\hat{\mathcal{H}}\{x\}(\omega) = \begin{cases} -j\cdot\hat{x}(\omega), & \omega > 0 \\ j\cdot\hat{x}(\omega), & \omega < 0. \end{cases} \tag{25}$$

Step 3.3) Thirdly, a value indicating comprehensive sparsity of each signal is computed using the above information. The sparsity indicator is defined as

$$\text{SparGroup}\{\boldsymbol{x}\} = K\{\boldsymbol{x}\}\cdot\text{sgn}\,(KE\{\boldsymbol{x}\} - T), \tag{26}$$

where T is a threshold value selected based on engineering experiences. In this paper, according to our expertise, this value was selected as 20. Moreover, in the procedure, only a finite frequency range of $\boldsymbol{x}$ is utilized. According to the results in the paper by He *et al.* [27], a feasible frequency range can be selected as $[1.5f_c,\ 3.5f_c]$.

Step 4) After obtaining all sparse indicator values of signals derived by TFMRA, we can plot them in a two dimensional

distribution diagram. A subspace with greatest sparsity estimation value is selected as the optimal feature. Plots regarding the time domain waveform, the Fourier spectrum and the instantaneous frequency/amplitude of the optimal feature are used to extract fault signatures. Other subspaces within the NCWPC containing the optimal feature, together with neighboring wavelet packets of these NCWPC, may also be useful as they can provide other fault information.

The improved indicator is devised based on the following facts. Firstly, evenly spaced spectral bins will appear in the envelope spectra of the reconstructed signals. It will result in high kurtosis value in the frequency domain. Secondly, envelope spectra of noises are comparatively flat in shape and thus produce low kurtosis values. Thirdly, for a sporadic impulse with extremely localized energy in the time domain, due to lack of periodicity, its envelope spectrum is also flat in shape, hence producing low kurtosis values. Proper selections of parameters in Equation (26) are very important to analysis results.

VI. EXPERIMENTAL VERIFICATION AND ANALYSIS OF EFFECTIVENESS

A. INTRODUCTION OF EXPERIMENT

In order to verify the effectiveness of the proposed method, a rub-impact experiment was conducted. The single span rotor test rig is shown in Figure 5. In the tests, incipient faulty components were produced by periodic contacts between the rubbing screw and the rotating shaft.

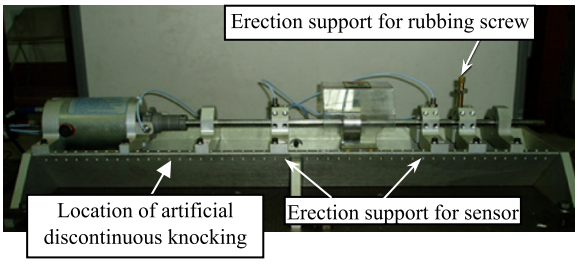

FIGURE 5. Photograph of the single span rotor test rig.

In the experiment, the rotation speed of the shaft was controlled at $2200r \cdot \min^{-1}$. The working frequency of the rotor system was theoretically calculated at 36.67Hz. On each side of the rotor there was an erection support for installing eddy current sensors (Figure 6(a)). At each erection support, each pair of eddy current sensors were mounted perpendicularly. The fault source was simulated by a rubbing screw (Figure 6(b)). When the rotor system was operating at constant speed, artificial knockings were made on the metal surface of the test rig in order to simulate stochastic sporadic impulses occurring in actual measurement.

B. PROCESSING RESULTS OF MEASURED SIGANL USING ORDINARY METHODS

In Figure 7, we plot the displacement signal collected from the eddy current sensor mounted in the X direction. In the

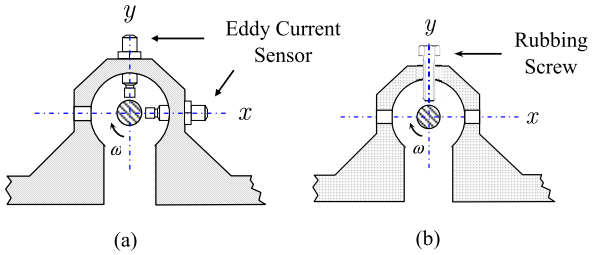

FIGURE 6. (a) Deployment of eddy current sensors; (b) installation of rubbing screw.

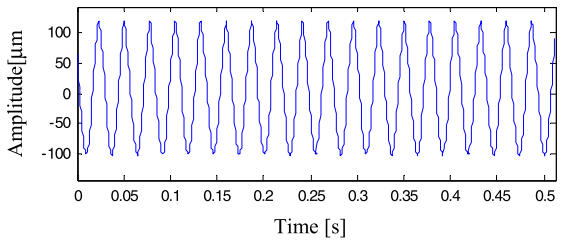

FIGURE 7. Time domain waveform of the displacement signal collected by the eddy current sensor.

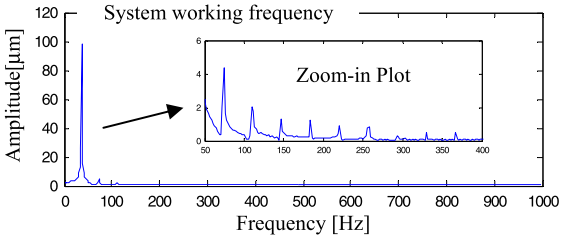

FIGURE 8. Frequency domain waveform of the displacement signal collected from the eddy current sensor.

measurement, the sampling frequency was set as 2000Hz and the sampling length was set as 1000. The waveform in the time domain shows that a sinusoidal wave related to the working frequency of the system (f_c) is the dominant component. Similarly, the amplitude of its associated spectral bin is of extremely high energy in the Fourier spectrum (Figure 8). From the zoom-in plot, we an observe the high order tones of f_c in the frequency range of [50,400]Hz.

Applying Hilbert transform on the original vibration signal shown in Figure 7, the curve of instantaneous frequency (IF) of the displacement signal is shown in Figure 9. The averaged value of IF in the time interval of [0.05,0.45]s is calculated at 36.7068Hz, very close to the theoretical value of system working frequency. The periodical oscillations of the IF curve are also important phenomena. At the time instant of t=0.1975s there is a special sudden frequency change. As stated above, this sudden change was caused by the artificial knocking.

C. SINGLE MODE COMPONENT EXTRACTION USING THE PROPOSED SMART METHOD

In this subsection, we illustrate processing results of the displacement signal by using the proposed smart method. The characteristic frequency of the rotor system is selected

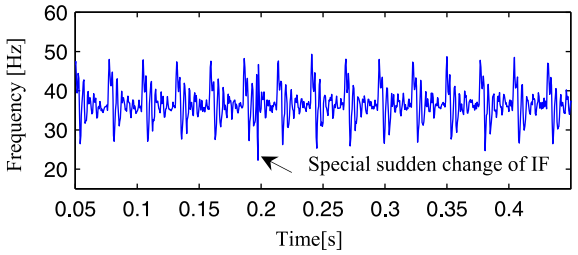

FIGURE 9. Change of the instantaneous frequency of the raw displacement signal.

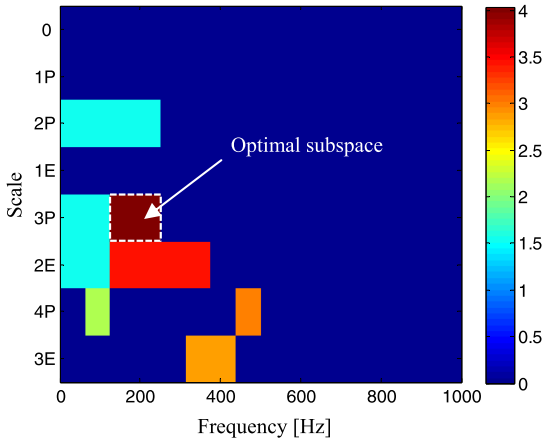

FIGURE 10. Distribution of the sparsity estimation indicators calculated from decomposition results of the raw vibration signal.

as $f_c = 36.7$Hz. As shown in Figure 10, the wavelet subspace $wp_3^2(t)$ (passing band: [125,250]Hz, central analyzing frequency: 187.5Hz) is recognized to possess the highest sparsity estimation value.

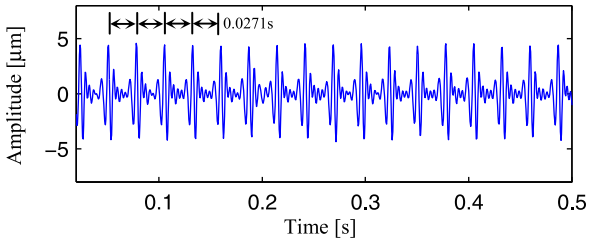

FIGURE 11. Time domain wave of the optimal subspace of the raw displacement signal.

The time domain waveform of the optimal wavelet subspace is plotted in Figure 11, in which periodical damping components spaced at 0.0271s are very prominent. The corresponding fault frequency is calculated at 36.68Hz. In consideration of permissible error range, this calculated frequency is much closed to the theoretical characteristic frequency. From the envelope spectrum shown in Figure 12, the fundamental tone, second order tone, and third order tone of the system working frequency are revealed as dominant components.

Comparing the diagrams in Figure 9 and Figure 11, we found occurrences of the damping components are in

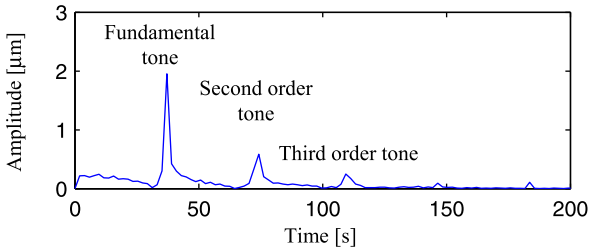

FIGURE 12. Envelope spectrum of the optimal subspace of the raw displacement signal.

significant synchronism with those of sudden IF changes. This phenomenon demonstrates the extracted fault features are actually produced by the rub-impact faults.

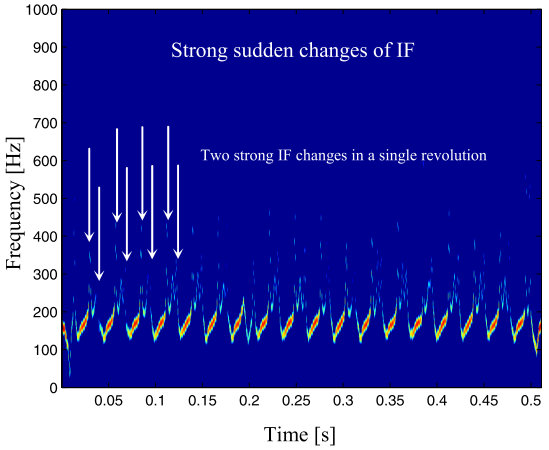

FIGURE 13. Instantaneous frequency of waveform of the optimal subspace signal.

In Figure 13, the IF of the extracted signal is plotted. In this figure, periodical IF changes are also found. The occurrence instants of the IF changes are also simultaneous with those of the original signal.

From zoom-in plots of Figure 13, it can be seen that two strong IF permutations are found in each revolution of the shaft, meaning that this signal may be composed of more than one vibration mode. Investigating the neighboring wavelet subspaces of the optimal wavelet subspace $wp_3^2(t)$, two wavelet subspace of significant modulation effect were found. The waveforms of the two wavelet subspaces, whose passing bands are [125,187.5]Hz and [187.5,312.5]Hz, were plotted in Figure 14 and Figure 15.

Implementing demodulation using Hilbert transform on the waveforms in Figure 14 and Figure 15, the corresponding IF cures are shown in Figure 16 and Figure 17 respectively. The sudden IF changes of the two curves happen simultaneously. In each revolution of shaft, there is only one strong IF change. What's more, judging from the IF change instants, it is inferred that the wavelet subspace characterized by [125,187.5]Hz contains a single vibration mode of amplitude modulation and the other wavelet subspace characterized by

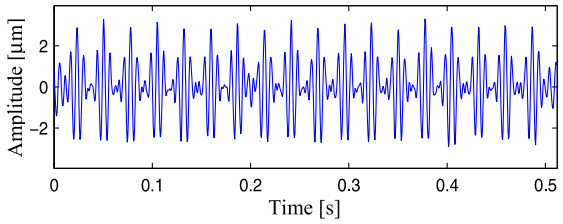

FIGURE 14. Time domain waveform of the wavelet subspace whose passing band is [125, 187.5]Hz.

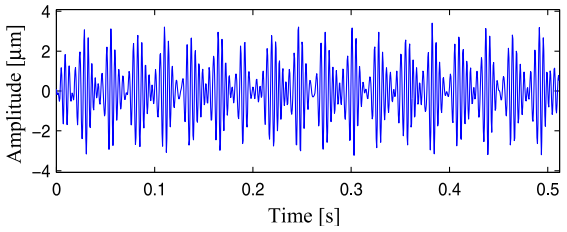

FIGURE 15. Time domain waveform of the wavelet subspace whose passing band is [187.5, 312.5]Hz.

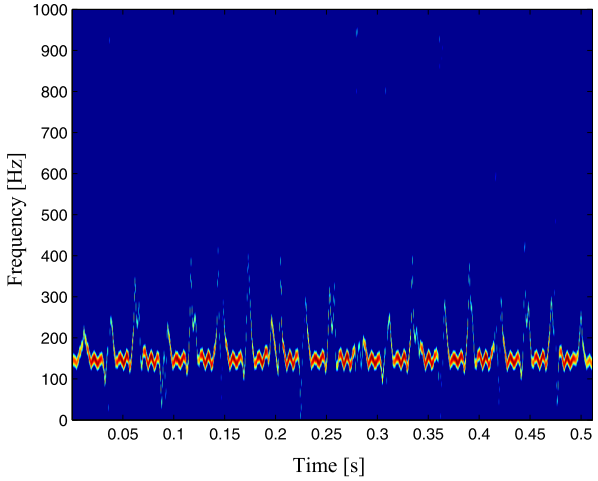

FIGURE 16. Instantaneous frequency cure of the wavelet subspace characterized by [125, 187.5]Hz.

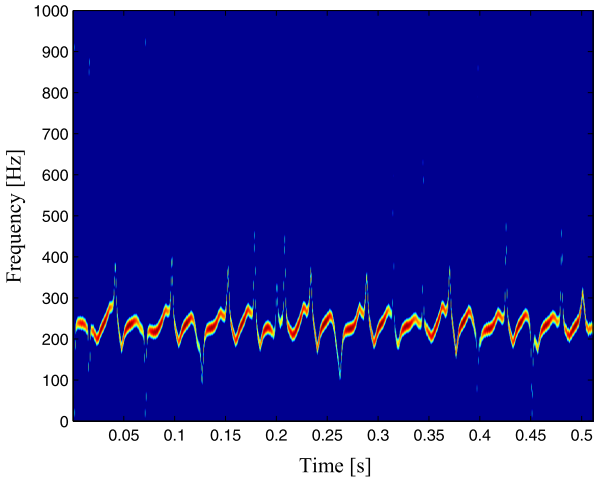

FIGURE 17. Instantaneous frequency cure of the wavelet subspace characterized by [187.5, 312.5]Hz.

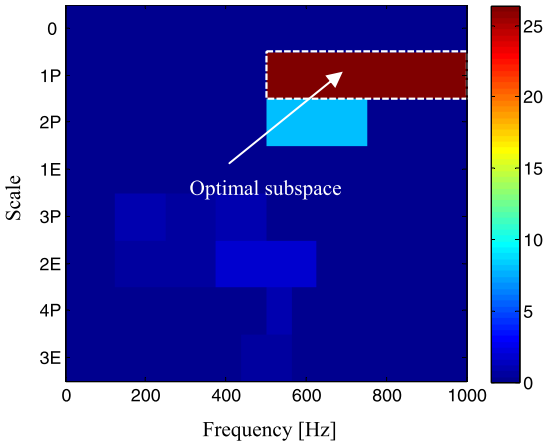

FIGURE 18. Processing results using a method which employs the indicator of spatial-spectral ensemble kurtosis.

[187.5, 312.5]Hz contains a single vibration mode of frequency modulation.

D. PROCESSING RESULTS BY COMPARISON METHODS

In order to demonstrate the superiority of the proposed method, we employed three other comparison methods to process the original displacement signal.

(1) Comparison with method using other fault feature sensitive indicator

As comparison, we employ another intelligent feature extraction method using an indicator named as spatial-spectral ensemble kurtosis [29]. The signal was also decomposed using the proposed TFMRA. The distribution of the sparsity indicator is shown in Figure 18. The wavelet subspace characterized by [500, 1000]Hz was recognized as the optimal wavelet subspace. Unfortunately, as shown in Figure 19(a), a component containing a sporadic impulse happening at t=0.1975s, was extracted. Such component was supposed to be suppressed by the indicator but failed in doing so. This strong impulse produces a high kurtosis value of 8 in the time domain.

The component containing the sporadic impulse was successfully suppressed by the proposed method. As shown in Figure 19(b), the envelope spectrum of this component is flat in shape and produces low kurtosis value in this domain. Therefore in the proposed method, due to the threshold processing in Equation (26), interferences caused by the sporadic impulse are removed.

In order to locate the source of the sporadic impulse in the time domain, in Figure 20 we display a zoom-in plot of the original displacement signal. At the time instant of 0.1975s, a singularity of small energy was found. However, compared with energy of the dominant sinusoidal wave related to the system working frequency, the singularity is so weak in energy that we hardly recognize it in the time domain without zoom-in operations.

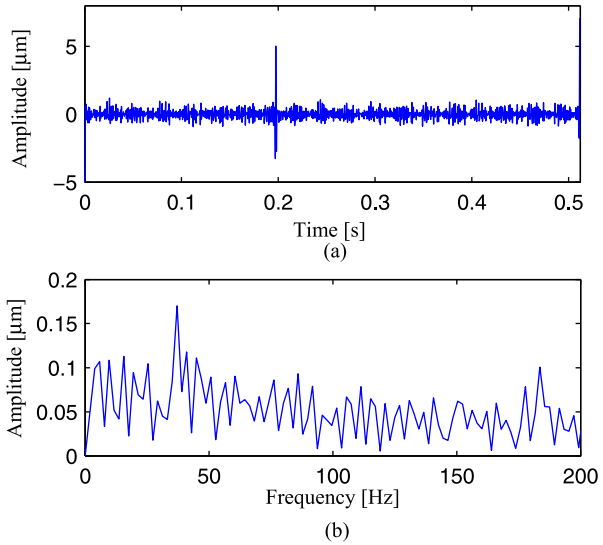

FIGURE 19. Information of the optimal subspace in Figure 18: (a) time domain waveform; (b) envelope spectrum.

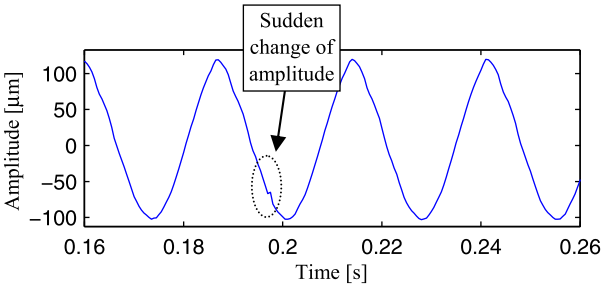

FIGURE 20. Sporadic impulse (caused by artificial knocking) in the time domain.

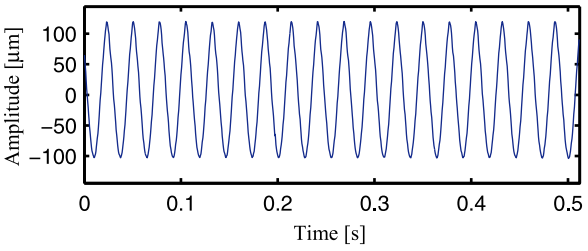

FIGURE 21. Processing results by group sparsity technique.

(2) Comparison with a group sparsity technique

Group sparsity is reported to be an advanced technique to extract periodic impulsive components in the presence of observation noises [29], [31]. The pre-required knowledge of this technique is also the system characteristic frequency. The processing results are shown in Figure 21. The denoised signal after processing is also similar to the raw displacement signal in shape. Owing to the strong interferences caused by the dominant system working frequency, the repetitive impulses were not identified despite this comparison technique employs stronger non-convex regularizer.

(3) Comparison with TQWT based resonance sparse signal decomposition

Tunable Q-factor wavelet transform is a new type of wavelet dictionary whose time-frequency atoms can be parameterized by quality factor (Q), redundant factor (r) and decomposition stage (J). Resonance sparse signal representation based on TQWT emerges as an effective way to separate fast varying components and slow varying components from single sensor observations [26], [32]. In this paper, for the fast varying wavelet dictionary the parameters were chosen as Q=4 and r=3, while for the slow varying wavelet dictionary the parameters were chosen as Q=1 and r=3. The processing results are shown in Figure 22. Similar to the case of group sparsity technique, owing to the presence of harmonic wave of extremely high energy, both of the extracted fast varying component (Figure 22(a)) and the extracted slow varying component (Figure 22(b)) are very similar to the original displacement signal in shape. Using other parameter combinations $\{Q,r,L\}$ for the two dictionaries, results are similar to those in Figure 22.

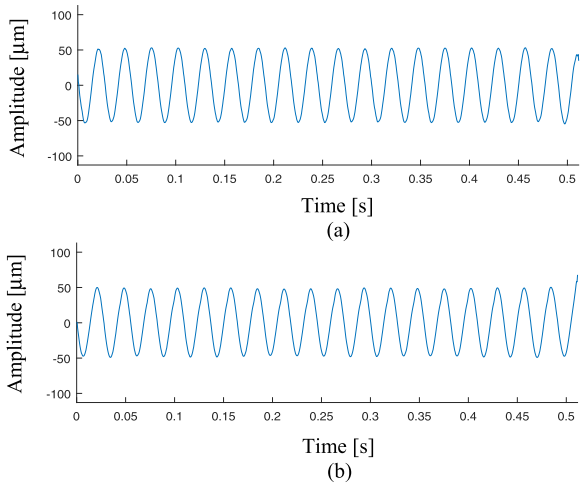

FIGURE 22. Processing results by TQWT based resonance sparsity decomposition technique: (a) fast varying component; (b) slow varying component.

Based on the comparison demonstrated above, due to the interferences in the raw displacement signal, the comparison method based on sparse representation fail in extracting incipient periodic impulsive transients in the experiment. These comparisons demonstrate the superiority of the proposed method in overall performance.

VII. CONCLUSION

In order to enhance the fault diagnosis performance in investigating vibration signal containing multiple modes, we propose a smart technique based on the combination of TFMRA and an improved sparsity promoted indicator. TFMRA distinguish itself from classical wavelet theories by enabling continuous refinement of spectral resolution around specific central frequencies. Major findings of the paper are listed as below.

(1) On the basis of quasi-analytic wavelet packet transform, a novel theory of topological fractal multi-resolution analysis is proposed with concrete construction example. With the novel concept of nested centralized wavelet packet cluster, TFMRA is able to realize multi-target pursuit via multi-resolution analysis around specific spectral focuses. This merit has not been reported in the literature.

(2) We give rigorous mathematical proofs for the following properties of TFMRA: each NCWPC can be regarded as a topological subset of the frequency domain of the original signal; fractal sets can be constructed by NCWPCs. The intrinsic isomorphism between classical dyadic wavelet theory and TFMRA is also revealed. That is, each dyadic wavelet packet can be uniquely associated with a specific NCWPC according to definitions of TFMRA. In the framework of TFMRA, dyadic wavelet analysis can be regarded as a proper subset of TFMRA.

(3) A smart fault feature extraction method is put forward. Based on TFMAR and sparsity characteristics of periodic impulsive components in the envelope spectrum domain, it is able to suppress stochastic interferences as well as deterministic interferences more effectively. Combining the recognized optimal wavelet packet with its instantaneous information, we found it more feasible to identify vibration modes of complete physical meaning. A rub-impact experiment on a rotor test rig was used to verify the superiority of the proposed method.

REFERENCES

[1] G. Wang, Z. He, X. Chen, and Y. Lai, "Basic research on machinery fault diagnosis," *J. Mech. Eng.*, vol. 49, no. 1, pp. 64–72, 2013.

[2] W.-K. Chen, *Linear Networks and Systems*. Belmont, CA, USA: Wadsworth, 1993, pp. 123–135.

[3] H. D. M. de Azevedo, A. M. Araújo, and N. Bouchonneau, "A review of wind turbine bearing condition monitoring: State of the art and challenges," *Renew. Sustain. Energy Rev.*, vol. 56, pp. 368–379, Apr. 2016.

[4] W. Caesarendra, B. Kosasih, A. K. Tieu, H. Zhu, C. A. S. Moodie, and Q. Zhu, "Acoustic emission-based condition monitoring methods: Review and application for low speed slew bearing," *Mech. Syst. Signal Process.*, vols. 72–73, pp. 134–159, May 2016.

[5] K. Ding, M. Xie, and Z. J. Yang, *The Theory and Technology of Discrete Spectrum Correction*. Beijing, China: Science Press, 2008.

[6] R. Yan, R. X. Gao, and X. Chen, "Wavelets for fault diagnosis of rotary machines: A review with applications," *Signal Process.*, vol. 96, pp. 1–15, Mar. 2014.

[7] W. P. He, Y.Y. Zi, B. Q. Chen, B. Yao, and Z. S. Zhang, "Periodic sparsity oriented super-wavelet analysis with application to motor bearing fault detection of wind turbine," *J. Mech. Eng.*, vol. 52, no. 3, pp. 41–48, 2016.

[8] Y. Lei, J. Lin, Z. He, and M. J. Zuo, "A review on empirical mode decomposition in fault diagnosis of rotating machinery," *Mech. Syst. Signal Process.*, vol. 35, nos. 1–2, pp. 108–126, Feb. 2013.

[9] K. Dragomiretskiy and D. Zosso, "Variational mode decomposition," *IEEE Trans. Signal Process.*, vol. 62, no. 3, pp. 531–544, Feb. 2014.

[10] Y. Han, B. Tang, L. Deng, "Multi-level wavelet packet fusion in dynamic ensemble convolutional neural network for fault diagnosis," *Measurement*, vol. 127, pp. 246–255, Oct. 2018.

[11] H. Shao, H. Jiang, X. Li, and S. Wu, "Intelligent fault diagnosis of rolling bearing using deep wavelet auto-encoder with extreme learning machine," *Knowl.-Based Syst.*, vol. 140, pp. 1–14, Jan. 2018.

[12] Z. Huo, Y. Zhang, P. Francq, L. Shu, and J. Huang, "Incipient fault diagnosis of roller bearing using optimized wavelet transform based multi-speed vibration signatures," *IEEE Access*, vol. 5, pp. 19442–19456, 2017.

[13] Y. Qin, J. Zou, and F. Cao, "Adaptively detecting the transient feature of faulty wind turbine planetary gearboxes by the improved kurtosis and iterative thresholding algorithm," *IEEE Access*, vol. 6, pp. 14602–14612, 2018.

[14] Y. Liu, C. Yang, and Q. Sun, "Enhance embedding capacity of generalized exploiting modification directions in data hiding," *IEEE Access*, vol. 6, pp. 5374–5378, 2018.

[15] J.-L. Starck, M. Elad, and D. L. Donoho, "Image decomposition via the combination of sparse representations and a variational approach," *IEEE Trans. Image Process.*, vol. 14, no. 10, pp. 1570–1582, Oct. 2005.

[16] M. Elad, *Sparse and Redundant Representations: From Theory to Applications in Signal and Image Processing*. New York, NY, USA: Springer, 2010.

[17] Z. Feng and M. Liang, "Complex signal analysis for planetary gearbox fault diagnosis via shift invariant dictionary learning," *Measurement*, vol. 90, pp. 382–395, Aug. 2016.

[18] W. He, Y. Zi, Z. Wan, and B. Chen, "Improved ensemble superwavelet transform for vibration-based machinery fault diagnosis," *J. Manuf. Sci. Eng.-Trans. ASME*, vol. 138, no. 7, p. 071012, 2016.

[19] W. He, B. Chen, N. Zeng, and Y. Zi, "Sparsity-based signal extraction using dual Q-factors for gearbox fault detection," *ISA Trans.*, vol. 79, pp. 147–160, Aug. 2018.

[20] X. Fan, Q. Lian, and B. Shi, "Compressed sensing MRI with phase noise disturbance based on adaptive tight frame and total variation," *IEEE Access*, vol. 5, pp. 19311–19321, 2017.

[21] N. Zeng, H. Zhang, Y. Li, J. Liang, and A. M. Dobaie, "Denoising and deblurring gold immunochromatographic strip images via gradient projection algorithms," *Neurocomputing*, vol. 247, pp. 165–172, Jul. 2017.

[22] N. Zeng, H. Zhang, B. Song, W. Liu, Y. Li, and A. M. Dobaie, "Facial expression recognition via learning deep sparse autoencoders," *Neurocomputing*, vol. 273, pp. 643–649, Jan. 2018.

[23] W. Sun *et al.*, "Health state monitoring of bladed machinery with crack growth detection in BFG power plant using an active frequency shift spectral correction method," *Materials*, vol. 10, no. 8, p. 925, 2017, doi: 10.3390/ma10080925.

[24] P. Flandrin, G. Rilling, P. Goncalves, "Empirical mode decomposition as a filter bank," *IEEE Signal Process. Lett.*, vol. 11, no. 2, pp. 112–114, Feb. 2004.

[25] Y. Wang and R. Markert, "Filter bank property of variational mode decomposition and its applications," *Signal Process.*, vol. 120, pp. 509–521, Mar. 2016.

[26] G. Cai, X. Chen, and Z. He, "Sparsity-enabled signal decomposition using tunable Q-factor wavelet transform for fault feature extraction of gearbox," *Mech. Syst. Signal Process.*, vol. 41, nos. 1–2, pp. 34–53, 2013.

[27] W. He, Y. Zi, B. Chen, F. Wu, and Z. He, "Automatic fault feature extraction of mechanical anomaly on induction motor bearing using ensemble super-wavelet transform," *Mech. Syst. Signal Process.*, vols. 54–55, pp. 457–480, Mar. 2015.

[28] B. Chen, Z. Zhang, Y. Zi, and Z. He, "Novel ensemble analytic discrete framelet expansion for machinery fault diagnosis," *J. Mech. Eng.*, vol. 50, no. 17, pp. 78–86, 2014.

[29] B. Chen, Z. Zhang, Y. Zi, Z. He, and C. Sun, "Detecting of transient vibration signatures using an improved fast spatial–spectral ensemble kurtosis kurtogram and its applications to mechanical signature analysis of short duration data from rotating machinery," *Mech. Syst. Signal Process.*, vol. 40, no. 1, pp. 1–37, 2013.

[30] W. He, Y. Ding, Y. Zi, and I. W. Selesnick, "Repetitive transients extraction algorithm for detecting bearing faults," *Mech. Syst. Signal Process.*, vol. 84, pp. 227–244, Feb. 2017.

[31] W. He, Y. Ding, Y. Zi, and I. W. Selesnick, "Sparsity-based algorithm for detecting faults in rotating machines," *Mech. Syst. Signal Process.*, vols. 72–73, pp. 46–64, May 2016.

[32] W. Huang, H. Sun, and W. Wang, "Resonance-based sparse signal decomposition and its application in mechanical fault diagnosis: A review," *Sensors*, vol. 17, no. 6, p. 1279, 2017.

XINCHENG CAO was born in Weifang, Shandong, China, in 1992. He received the bachelor's and master's degrees in mechanical engineering from the School of Aerospace Engineering, Xiamen University, China, in 2015 and 2018, respectively, and the Ph.D. degree from the School of Aerospace Engineering, Xiamen University. His main research interests include intelligent equipment and smart manufacturing, and structural health monitoring of equipment.

NIANYIN ZENG was born in Longyan, Fujian, China, in 1986. He received the B.Eng. degree in electrical engineering and automation and the Ph.D. degree in electrical engineering from Fuzhou University in 2008 and 2013, respectively. From 2012 to 2013, he was an RA with the Department of Electrical and Electronic Engineering, The University of Hong Kong.

He has been a Visiting Professor with the Korea Advanced Institute of Science and Technology since 2017. He is currently an Assistant Professor with the Department of Instrumental and Electrical Engineering, Xiamen University. He has authored or co-authored several technical papers, including 5 ESI highly cited papers according to the most recent Clarivate Analytics ESI report. His current research interests include intelligent data analysis, computational intelligent, time-series modeling, and applications. He is a very active reviewer for many international journals and conferences. He is an ISEF Fellow founded by the Korea Foundation for Advance Studies.

Dr. Zeng also serves as a Technical Program Committee Member of ICBEB 2014 and an Invited Session Chair of ICCSE 2017. He is currently serving as an Associate Editor for *Neurocomputing* and also an Editorial Board Member for *Computers in Biology and Medicine*, *Biomedical Engineering Online*, *Journal of Advances in Biomedical Engineering and Technology*, and *Smart Healthcare*.

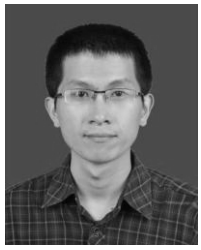

BINQIANG CHEN was born in Fuqing, Fujian, China, in 1986. He received the bachelor's degree in mechanical engineering from the School of Manufacturing Science and Technology, Sichuan University, in 2008, and the Ph.D. degree in mechanical engineering from the School of Mechanical Engineering, Xi'an Jiaotong University, in 2013. His main research interests include intelligent equipment and smart manufacturing, structural health monitoring of equipment, and applied harmonic analysis.

WANGPENG HE was born in Yulin, Shaanxi, China. He received the B.S. and Ph.D. degrees in mechanical engineering from Xi'an Jiaotong University, Xi'an, China, in 2007 and 2016, respectively. In 2014, he was appointed as a Visiting Scholar at the New York University, USA. He joined the School of Aerospace Science and Technology, Xidian University, where he is currently an Assistant Professor. His research interests include signal processing, machine vision, sparsity-based signal processing, and machinery fault diagnosis.